A holistic approach to interface stabilization for efficient perovskite solar modules with over 2,000-hour operational stability

doi: info:doi/10.1038/s41560-020-0653-2

A holistic approach to interface stabilization for efficient perovskite solar modules with over 2000 hour operation stability

Zonghao Liu†[1,2], Longbin Qiu†[1,3], Luis K. Ono[1], Sisi He[1], Zhanhao Hu[1], Maowei Jiang[1], Guoqing Tong[1], Zhifang Wu[1], Yan Jiang[1], Dae-Yong Son[1], Yangyang Dang[1], Said Kazaoui[4], Yabing Qi*[1]

[1]Energy Materials and Surface Sciences Unit (EMSSU), Okinawa Institutes of Science and Technology Graduate University (OIST), 1919-1 Tancha, Onna-son, Kunigami-gun, Okinawa 904-0495, Japan

[2]Wuhan National Laboratory for Optoelectronics, Huazhong University of Science and Technology, Wuhan 430074, Hubei, China

[3]Department of Mechanical and Energy Engineering, Southern University of Science and Technology, Shenzhen 518055, Guangdong, China

[4]Research Center for Photovoltaics (RCPV), National Institute of Advanced Industrial Science and Technology (AIST), Tsukuba, Japan

† These authors contribute equally to this work.

*Corresponding author: Yabing Qi, E-Mail: Yabing.Qi@OIST.jp

Upscaling of perovskite solar cells to module scale and affording long-term stability have been recognized as the most important challenges for commercialization of this emerging photovoltaic technology. In a perovskite solar module (PSM), each interface within the device contributes to the efficiency and stability. Here, we employ a holistic interface stabilization strategy by modifying all the relevant layers and interfaces, namely the perovskite layer, charge transporting layers and the device encapsulation to improve the efficiency and stability of PSMs. The treatments were selected to be compatible with low-temperature scalable processing and the module scribing steps. Our unencapsulated PSM achieved a reverse-scan efficiency of 16.6% with a designated area of 22.4 cm^2. The encapsulated PSM retained approximately 86%

of the initial performance after continuous operation for 2000 h under AM 1.5G light illumination, with translates into a T_{90} lifetime of 1570 h and an estimated T_{80} lifetime of 2680 h.

Introduction

In the past decade, small-size perovskite solar cells (PSCs) with an active area of ~ 0.1 cm^2 have achieved outstanding power conversion efficiencies (PCE) over 25%.[1] For practical applications, PSCs must retain high efficiency when up-scaled. However, when their size was increased to module scale with active area above 10 cm^2 the efficiency decreased significantly. The efficiency of 10-cm^2 perovskite solar modules (PSMs) is currently in the range of 10 ~ 17%.[2-4] As the PCE is still much lower than that of commercialized solar modules based on other photovoltaic technologies it is desirable to further improve the PSMs efficiency.

Besides up-scalability and efficiency, the long-term stability of PSMs is another important aspect for their practical application.[5,6] In particular, the device operation stability under continuous illumination is an important indicator of the long-term stability of PSCs, as well as PSMs.[5,7-9] To improve the continuous operation stability of PSCs, the engineering of the individual functional layer and the relevant interfaces including perovskite layer[10-14], electron transport layer (ETL)[15], hole transport layer (HTL)[16], counter electrode (CE)[17] and encapsulation layer[18] has been developed in separate works. Although fine control of each interface has been proven to be of chief importance for the photovoltaic performance of PSCs, similar interface engineering strategies have not been widely considered and systematically investigated in the context of PSMs. This has been proposed to be the main reason why the PSCs stability reduce quickly when scaling up.[2,4] It is thus desirable to transfer the accumulated successful experiences in PSCs to PSMs.

Since each functional layer in a PSM contributes to its efficiency and stability, a holistic approach to the optimization of the interfaces of each functional layer throughout the entire device must be employed rather than the engineering of an

individual interface. However, the structure of PSMs is complex compared to small-area cells due to the series connections of multiple sub-cells and P1-P2-P3 interconnection structures. The interface engineering strategies employed in lab-scale PSCs that work for small-area cell are not always trivial to transfer to PSMs. For example, TiO_2 ETL has played a pivotal role in high-efficiency PSCs, but if one does not remove TiO_2 in the P2 patterning step for PSM, the relatively high resistance of TiO_2 will cause a substantially lower FF.[19,20] Besides, the exposure of P2 and P3 patterning lines also increase the possibility for external stressor induced degradation.[21] Therefore, a holistic approach to PSM design that considers the process compatibility with scalable production as well as the module structure and encapsulation is essential for transferring the strategies of PSCs to PSMs.

Here, we report a holistic interface stabilization (HIS) strategy that takes into consideration the engineering of all the relevant interfaces in a perovskite solar device at the module scale. More specifically, we stabilize the SnO_2 ETL with ethylenediaminetetraacetic acid dipotassium (EDTAK), reduce the defects in the perovskite surface with an ethylammonium iodide (EAI) treatment, inhibit the moisture ingress and Au migration into the 2,2',7,7'-tetrakis[N,N-bis(p-methoxyphenyl)amino]-9,9'-spirobifluorene (spiro-OMeTAD) HTL with the incorporation of poly(3-hexylthiophene) (P3HT) and ensure an effective device encapsulation with a parylene film. These treatments are not only compatible with scalable processing but also with scribing steps. Our HIS strategy leads to not only PSMs efficiency improvement, but also stability enhancement. The PSMs without encapsulation achieved a reverse-scan efficiency of 16.6% with a designated area of 22.4 cm^2. The encapsulated PSM with the best stability gave T_{90} and T_{80} operation stability lifetime of 1570 h and 2680 h, respectively, under AM 1.5G light illumination test.

Holistic interface stabilization approach

We adopt an indium tin oxide (ITO)/SnO_2/$Cs_{0.05}FA_{0.54}MA_{0.41}Pb(I_{0.98}Br_{0.02})_3$ (FA is formamidinium, MA is methylammonium)/spiro-OMeTAD/Au configuration as the basis to fabricate PSMs.[22,23] To improve both efficiency and stability, we devise an HIS strategy that optimize all the relevant layers and interfaces from the bottom ETL layer to the top encapsulation layer as shown in Figure 1. We consider the compatibility of each individual interface modification with the other modifications, with the PSM design and with the scalable manufacturing. Such integrated approach should facilitate the future transfer of the optimized device design to practical manufacturing processes.

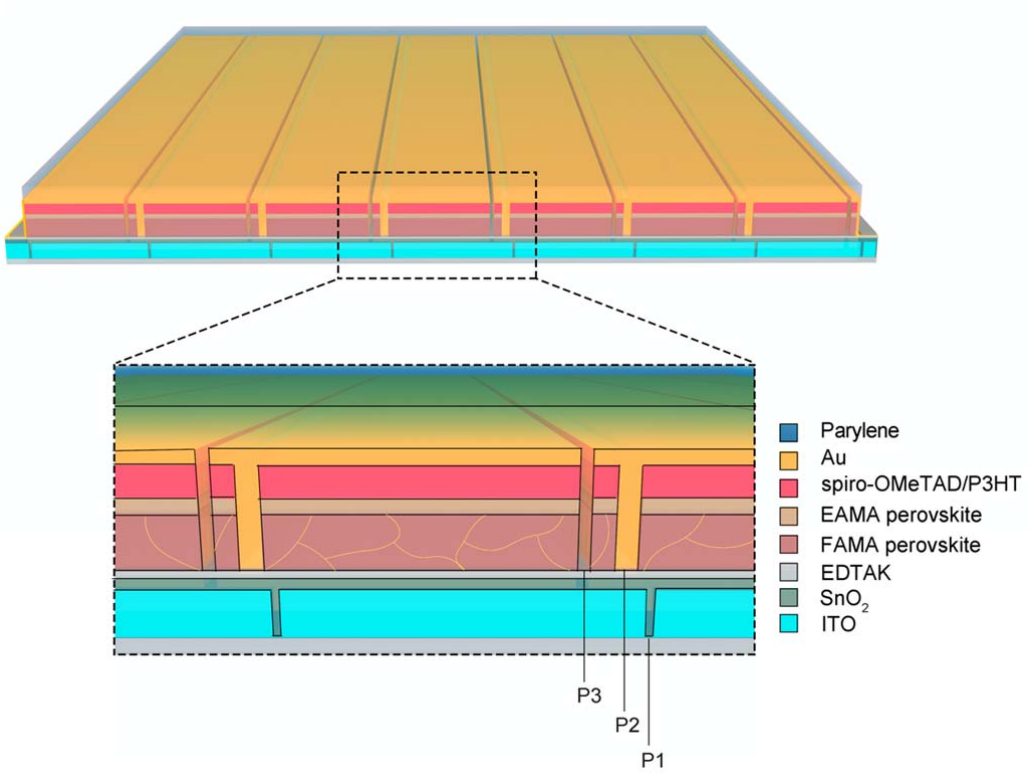

Figure 1 Holistic interface stabilization (HIS) strategy for PSMs. The HIS strategy consists of four treatments for the main device layers and their interfaces: the use of EDTAK to modify SnO_2; the use of EAI/MAI to form the EAMA-based perovskite on the surface of $Cs_{0.05}FA_{0.54}MA_{0.41}Pb(I_{0.98}Br_{0.02})_3$ (FAMA based perovskite); the incorporation of P3HT into the spiro-OMeTAD layer; the employment of the parylene encapsulation.

Regarding ETL and ETL/perovskite interface, we employ a commercial SnO_2 as ETL to take advantage of its efficient electron-selective properties[24], and its

compatibility with low-temperature and scalable coating process[22]. The use of approximately 20 nm-thick SnO_2 layer also enables a low resistance of P2 interconnection to ensure low series resistance and high fill factor.[19,25] Furthermore, we use EDTAK to mitigate the reaction of OH^- in SnO_2 with perovskite and tune the energy-level alignment at the ETL/perovskite interface. This modification also has negligible influence on the conductivity of the SnO_2 layer, which is important to ensure high-quality interconnection with low series resistance between each sub-cell in PSMs.

Regarding the perovskite/HTL interface, we use EAI/MAI surface treatment to passivate the surface defects of $Cs_{0.05}FA_{0.54}MA_{0.41}Pb(I_{0.98}Br_{0.02})_3$ perovskite (PVSK) and tune the energy-level alignment at this interface. The formed EAMA-perovskite could also reduce the influences from moisture in both top surface region and the regions related to wiring and encapsulation.

We then incorporate P3HT into the spiro-OMeTAD layer to induce a stable HTL against moisture and Au migration during device operation and P2 cutting process.[21]

These steps, the coating of SnO_2 with EDTAK followed by the deposition of the perovskite layer and the subsequent EAI/MAI treatment as well as the deposition of the HTL are highly compatible with scalable coating processes developed for organic and dye-sensitized solar modules.[2,4]

On the top of metal electrode, parylene encapsulation was made via upscalable chemical vapor deposition. Parylene encapsulation acts as a uniform and robust barrier layer, which helps keep the whole module including the P2 and P3 patterning lines into a closed space to prevent diffusion of external ambient gases such as moisture and oxygen, and contain the internally generated volatile degradation products.[26]

Stabilization of the ETL/perovskite interface

A stable ETL/perovskite contact and suitable energy-level alignment at this interface is essential for efficient and stable PSCs. The first step of our HIS strategy is to mitigate the reaction of OH^- in SnO_2 with perovskite (Supplementary Figure 1 and Supplementary Note 1) to form a stable ETL/perovskite interface by using EDTAK to

post-treat the SnO_2 layer on the basis of the acid-base neutralization reaction. The use of EDTAK also retained the positive passivation effect of K^+.[22] The treatment condition was optimized by changing the EDTAK concentration (Supplementary Table 1).

The observed N 1*s* peak in X-ray photoelectron spectroscopy (XPS) results in Figure 2a confirms the existence of EDTAK on the surface of the EDTAK treated SnO_2 (SnO_2-EDTAK) films. By immersing the SnO_2-EDTAK sample and pristine sample (SnO_2) into water and testing the pH value of the obtained aqueous solution, the pH value is slightly alkaline for the control sample, and neutral for the SnO_2-EDTAK sample. Based on the above observation, the reaction of KOH with perovskite is believed to be effectively mitigated by the EDTAK treatment.

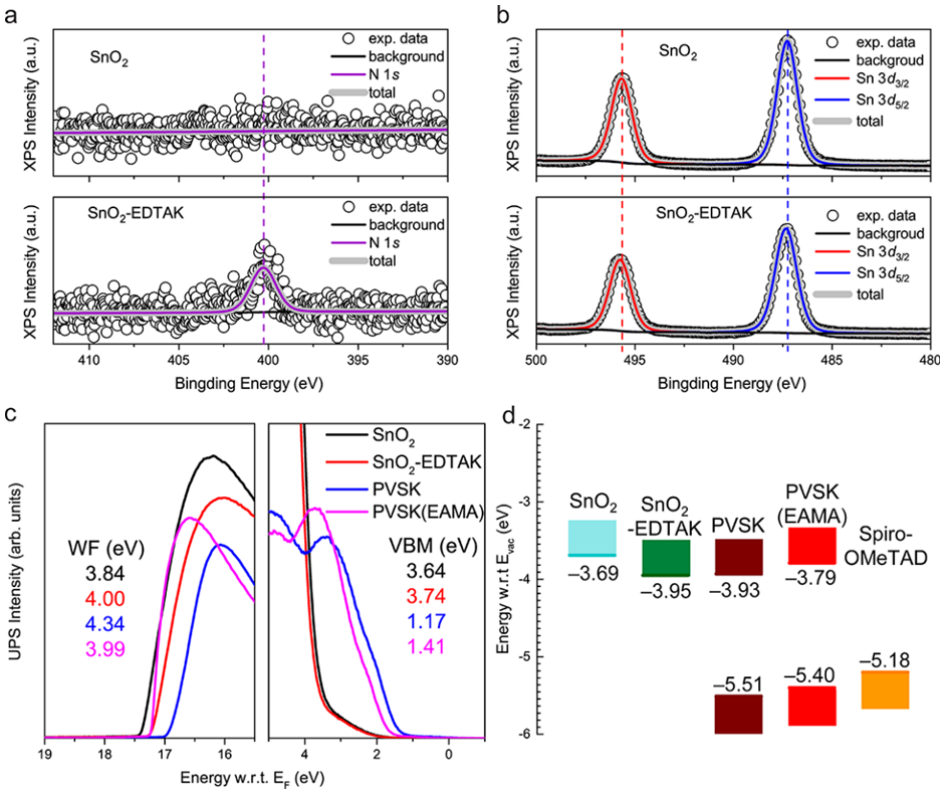

Figure 2 ETL/perovskite and perovskite/HTL interface stabilization and energy-level alignment. a-b, The N 1*s* spectra (**a**) and Sn 3*d* spectra (**b**) of SnO_2 and SnO_2-EDTAK films measured by XPS measurements. In (**a**) and (**b**), black circles show the original XPS data, black curves represent the background, the grey bold curves show the total fitting results. In (**a**), the purple vertical dash line shows the N 1*s* position with respect to SnO_2-EDTAK, the purple curves are the fitting results of

N1*s* signal. In (**b**), the red and blue vertical dash line show the Sn $3d_{3/2}$ and Sn $3d_{5/2}$ position, respectively, with respect to pristine SnO_2, the red and blue curves are the fitting results of Sn $3d_{3/2}$ and Sn $3d_{5/2}$ signal, respectively. **c**, UPS spectra (using the He-I line with a photon energy of 21.22 eV) corresponding to the secondary electron onset region and valence band maximum (VBM) of SnO_2, SnO_2-EDTAK, perovskite (PVSK), EAI/MAI-treated perovskite (PVSK(EAMA)) with respect to the Fermi energy (E_F). VBM for perovskites was determined from the semi-log plots (Supplementary Figure 3). **d**, Diagram of the energy levels of the materials as extracted from the UPS data.

Unlike a previous study[27] using EDTA as a pretreatment modifier to modify the SnO_2 colloidal solution, in the current work EDTAK is used as an interface post-treatment modifier to tune the energy-level alignment at the ETL/perovskite interface.[28] To investigate this point, XPS and ultraviolet photoemission spectroscopy (UPS) measurements were conducted. The observed slight shift of the Sn 3*d* peaks of SnO_2-EDTAK with respect to SnO_2 (Figure 2b) suggests a chemical interaction of EDTAK with SnO_2, which is likely to affect the energy-level alignment at the ETL/perovskite interface. As shown in Figure 2c, the work function (WF) of pristine SnO_2 and SnO_2-EDTAK is determined to be 3.84 eV and 4.00 eV, respectively. On the basis of our UPS and XPS analysis, EDTAK most likely act as interface modifier leading to variations in the WF of SnO_2-EDTAK, while minimum changes are observed for VBM and XPS Sn 3*d* core levels (see Supplementary Figure 2 and Supplementary Note 2).

The conduction band minimum (CBM) of the pristine SnO_2 was calculated to be −3.69 eV (with respect to the vacuum level E_{vac}), in agreement with reported values.[24,25] The CBM of SnO_2-EDTAK film shifts downward by about 0.26 eV with respect to the pristine SnO_2 film, which was calculated to be −3.95 eV. The improved energy-level alignment with CBM (−3.93 eV) of the perovskite (Figure 2d and Supplementary Figure 3) is expected to be beneficial for charge extraction at perovskite/ ETL interface.

To verify this, time resolved photoluminescence (TRPL) measurements were conducted (Supplementary Figure 4). The faster quench of perovskite PL for

181 SnO_2-EDTAK versus SnO_2 indicates a faster charge transfer from perovskite to
182 SnO_2-EDTAK.

183 We also used secondary ion mass spectrometry (SIMS) measurements to
184 investigate whether K^+ in EDTAK-SnO_2 can migrate into the perovskite film
185 (Supplementary Figure 5). The SIMS result confirms that the K^+ is distributed in both
186 perovskite bulk film and in the EDTAK-SnO_2 film. The K^+ [22,29] and Lewis base of the
187 alkylamine group[30] in EDTAK-SnO_2 could passivate perovskite defects, which is
188 supported by the longer PL lifetime of the glass/EDTAK/perovskite sample versus the
189 glass/perovskite sample (Supplementary Figure 4 and Supplementary Table 2).

190 To study the effect of the EDTAK treatment on device performance, small-size
191 PSCs were fabricated (Supplementary Figure 6). The current density-voltage (J-V)
192 curves of the devices based on pristine SnO_2 and EDTAK-SnO_2 are shown in Figure
193 3a. The pristine SnO_2 based PSCs (denoted as SnO_2/PVSK/spiro-OMeTAD/Au) show
194 a typical PCE of 19.2% with a short-circuit current density (J_{SC}) of 23.2 mA cm^{-2}, an
195 open-circuit voltage (V_{OC}) of 1.07 V, and a fill factor (FF) of 77.6%. EDTAK-SnO_2
196 based PSCs show a J_{SC} of 23.2 mA cm^{-2}, a V_{OC} of 1.10 V and a FF of 78.4%, leading
197 to an improved PCE of 20.1% with suppressed hysteresis (Supplementary Table 3). As
198 shown in Figure 3b, the representative external quantum efficiency (EQE) of
199 SnO_2-EDTAK device shows slightly higher values than the SnO_2 device at both the
200 short-wavelength and long-wavelength region, leading to a slightly higher integrated
201 Jsc for the former case (22.8 mA cm^{-2} versus 22.4 mA cm^{-2}). The improved Jsc as
202 well as improved V_{OC} and FF are likely due to dual function of the EDTAK treatment,
203 i.e., improvement of charge transport and suppression of charge recombination as
204 discussed above.

205 **Stabilization of the perovskite/HTL interface**

206 The second interface stabilization step is focused on the perovskite/HTL interface.
207 The higher defect density at the perovskite surface, especially at the surface grain
208 boundaries, with respect to the perovskite/ETL interface usually affects device
209 performance and stability significantly.[14,31] Here, interface stabilization with

EAI/MAI modification is adopted on the surface of perovskite to passivate defects as well as to enhance the device stability due to the robust stability of the EAMA based perovskite[32-34]. With respect to long-alkyl or other large-size ammonium-based cations, EA^+ has a relative smaller size, which favors the formation of quasi-3D perovskite even with a relative high EA content (Supplementary Note 3, Supplementary Figure 7-9 and Supplementary Table 4).[35-37]

To check the effect of the EAI/MAI treatment on the device performance (Supplementary Figure 10), small-size PSCs were fabricated, a typical J-V curve is shown in Figure 3a. The devices with both EDTAK and EAI/MAI treatment (denoted as SnO_2-EDTAK/PVSK(EAMA)/spiro-OMeTAD/Au, PVSK(EAMA) is $Cs_{0.05}FA_{0.54}MA_{0.41}Pb(I_{0.98}Br_{0.02})_3$ perovskite with the EAI/MAI treatment) show a typical PCE of 21.8% with a J_{SC} of 23.6 mA cm^{-2}, a V_{OC} of 1.12 V, and a FF of 82.3%. Based on EQE result in Figure 3b, the integrated current density is calculated to be 23.3 mA cm^{-2}, which is consistent with J_{SC} obtained from the J-V curve. This value is also higher than that of the device without treatment (SnO_2/PVSK/spiro-OMeTAD/Au) and device with EDTAK treatment (SnO_2-EDTAK/PVSK/spiro-OMeTAD/Au). Especially, the device with both EDTAK and EAI/MAI treatment shows higher EQE values at the long-wavelength region than that of device with EDTAK treatment. Considering that long-wavelength light is mainly absorbed by the perovskite near the perovskite/HTL interface. The improved current density is proposed attributed to the passivation effect of EAI/MAI treatment. Besides, the improved FF and V_{OC} also contribute to significantly improved PCE from 20.1% to 21.8% with EAI/MAI treatment.

To verify the passivation effect of EAI/MAI treatment, we used TRPL to investigate the charge carrier properties of the perovskite with and without EAI/MAI treatment (Figure 3c and Supplementary Table 5). The EAI/MAI treated perovskite sample showed a much longer PL lifetime than that of the untreated perovskite sample (122.4 ns versus 42.8 ns), which is likely the result of a reduction in nonradiative recombination by defect passivation via the EAI/MAI treatment. The defect density

reduction from 0.86×10^{16} to 0.47×10^{16} cm^{-3} measured by space-charge-limited current (SCLC) test further confirms the passivation effect of the EAI/MAI treatment (Figure 3d and e and Supplementary Note 4).

In addition, the EAI/MAI treatment affects the energy-level alignment at the perovskite/HTL interface. As shown in Figure 2c and d, the WF of EAI/MAI treated perovskite and untreated perovskite is determined to be 3.99 eV and 4.34 eV, respectively. The VBM is determined to be 1.41 eV and 1.17 eV, respectively, yielding the ionization energy value of 5.40 eV and 5.51 eV for perovskite with and without EAI/MAI treatment, respectively. The relative energy level position of the Fermi level shift also indicates a more *n*-type nature for the top surface of perovskite after the EAI/MAI treatment (Figure 2c, 2d, and Supplementary Figure 3), which is likely to originate from the partial change of the lead halide rich surface to a more organic halide rich surface induced by the EAI/MAI treatment.[38]

The mismatch of the energy-level alignment between perovskite and spiro-OMeTAD (ionization energy, 5.18 eV[39]) is reduced from 0.33 eV to 0.22 eV after the EAI/MAI treatment, which may benefit charge extraction at the perovskite/HTL interface. A faster quenching of perovskite PL for the PVSK(EAMA)/spiro-OMeTAD in comparison with PVSK/spiro-OMeTAD sample measured by TRPL (Figure 3c and Supplementary Table 5), further suggests that faster charge transfer occurs from EAI/MAI treated perovskite to spiro-OMeTAD. This also contributes to the suppressed hysteresis for the PSCs with both EDTAK and EAI/MAI treatment versus the PSCs with EDTAK treatment (Supplementary Table 3).

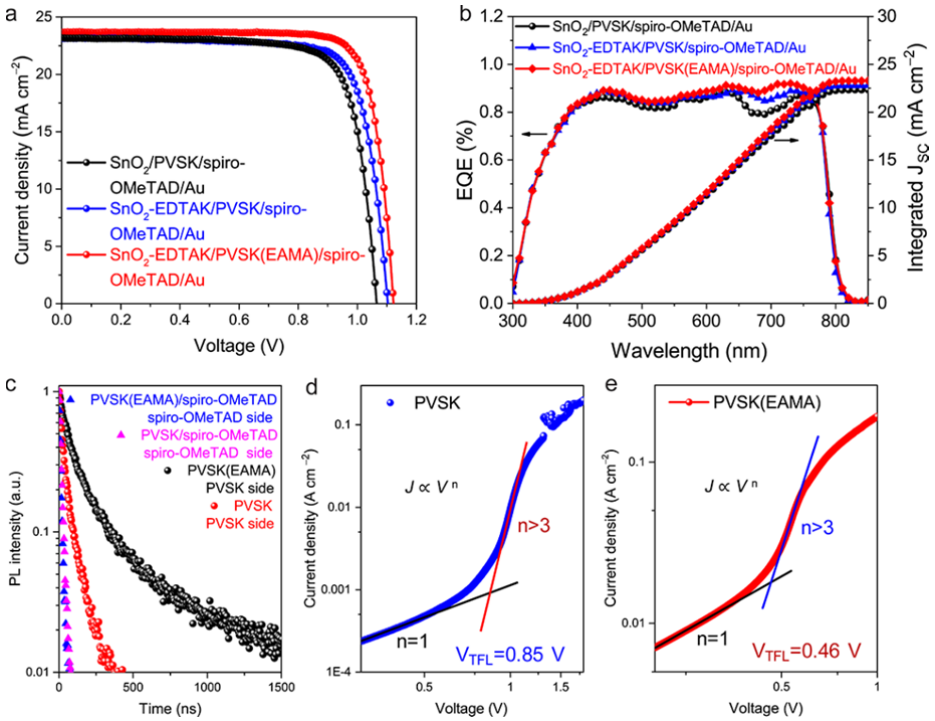

Figure 3 PSCs performance with ETL/perovskite and perovskite/HTL interface stabilization treatments and passivation effect of EAI/MAI treatment. **a**, J-V curves and **b**, EQE spectra and integrated J_{SC} of the PSCs treated with both EDTAK and EAI/MAI (red curve), treated with EDTAK (blue curve) and without treatments (black curve). **c**, TRPL decay curves of the perovskite thin film with (blue and black curves) or without (pink and red curves) EAI/MAI treatment as bare film (black and red curves) or interfaced with spiro-OMeTAD (blue and pink curves). **d-e**, J−V characteristics of SCLC result. The J-V curve can be fitted according to $J \propto V^n$ with different values of the exponent n: n = 1 is the ohmic region (dark fitted lines in (**d**) and (**e**)); n > 3 is the trap-filled limited (TFL) region (red fitted line and blue fitted line in (**d**) and (**e**), respectively). The TFL voltage (V_{TFL}) is onset voltage of the TFL region.

To further explore how the EAI/MAI treatment affects the perovskite film stability, the morphology of the perovskite with and without EAI/MAI treatment is measured by scanning electron microscopy (SEM) (Figure 4a-b). The grain boundaries are filled with additional structure for the EAI/MAI treated perovskite film with reduced roughness from 27.4 to 19.7 nm confirmed by atomic force microscopy (AFM) measurements (Figure 4c-d).

It has been reported that perovskite decomposition mainly starts from grain boundaries due to the relatively weak chemical binding and severe ion migration.[14,31]

The newly formed EAMA perovskite is thus expected to improve the perovskite stability due to passivation of grain boundaries. To verify this, the perovskite films are further subjected to high-energy electron beam with a voltage of 20 kV under SEM measurements (Supplementary Figure 11). Obvious cracks are observed for the untreated perovskite film, while the EAI/MAI treated perovskite film remains densely packed grain, which indicates an enhanced stability of latter case.[30]

To further study the perovskite stability, the perovskite films with and without EAI/MAI treatment are subject to a high relative humidity close to 100% at approximately 40 ^{o}C by monitoring the XRD evolution (Figure 4e-f). The PbI_2 peak in the untreated perovskite film shows much faster increase than that in the EAI/MAI treated perovskite film, which indicates slower degradation of EAI/MAI treated perovskite. The 85 ^{o}C thermal aging test of the films in a dry N_2 glove box also suggests the improved stability of EAI/MAI treated perovskite film (Supplementary Figure 12). These XRD observations together with the above morphology study coincidently suggest that the stability of perovskite film can be improved via EAI/MAI treatment.[31]

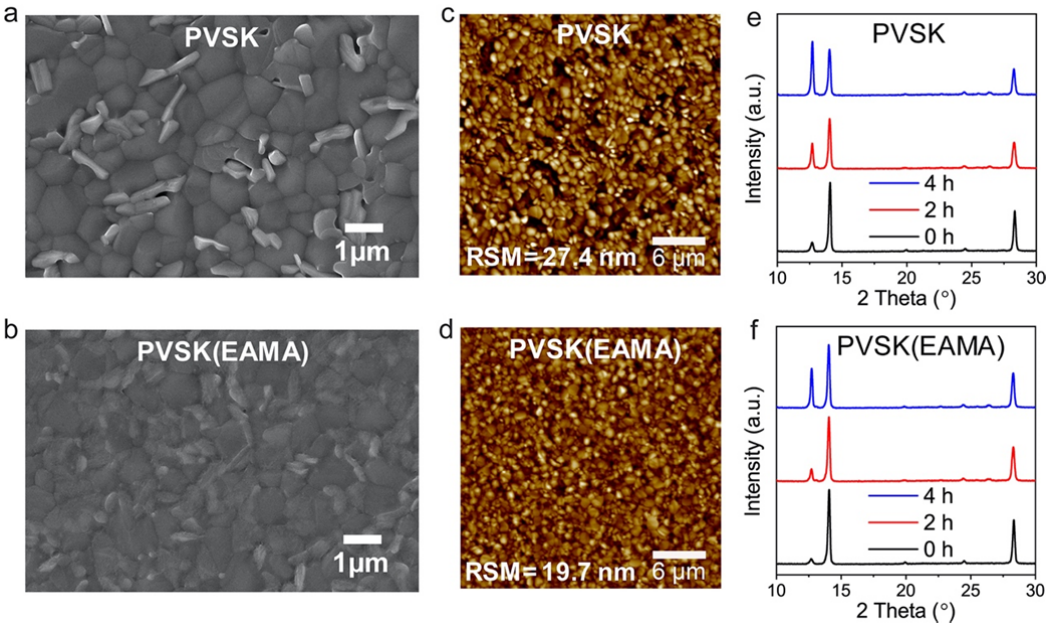

Figure 4 Perovskite film stability with perovskite/HTL interface stabilization. **a-b** Surface SEM images of the perovskite films without (PVSK) (**a**) and with (PVSK(EAMA)) (**b**) EAI/MAI treatment. **c-d**, AFM topography of the perovskite films without (**c**) and with (**d**) EAI/MAI treatment, RSM is root mean squared surface

roughness. **e-f**, XRD patterns evolution of the perovskite films without (**e**) and with (**f**) EAI/MAI treatment under aging test in a high relative humidity close to 100% condition at approximately 40 ^{o}C.

To apply the above studied interface stabilization strategy into large-scale device, PSMs were fabricated based on mirror-like and uniform large-area perovskite films (Supplementary Figure 13). Figure 5a shows the optical image of the PSM and Figure 5b shows the J-V curves of the PSMs with a designated area of 22.4 cm^2 obtained from reverse scan.

Consistent with the PSCs performance, the PSM with both EDTAK and EAI/MAI treatment (SnO_2-EDTAK/PVSK(EAMA)/spiro-OMeTAD/Au) showed substantially better performance (Supplementary Table 6). A champion module with both EDTAK and EAI/MAI treatment show a reverse-scan PCE of 16.6%, which corresponds to an active-area-efficiency of 18.2% (Supplementary Figure 14). To confirm our J-V results, we sent our module to National Institute of Advanced Industrial Science and Technology (AIST) for J-V characterization according to their standard protocol IEC60904-3 Ed. 3 (Supplementary Figure 15). The result is relatively consistent with our in-house measurements (Supplementary Figure 16).

The PSMs with both EDTAK and EAI/MAI treatment also exhibit good reproducibility (Supplementary Figure 17, Supplementary Table 7) and a small hysteresis (Supplementary Figure 18). To study the operation stability of above PSMs without encapsulation, we tracked the operation stability at a fixed bias that was set to be the initial MPP voltage under continuous AM 1.5G light illumination in a N_2 box with a relative humidity <5% (Figure 5c). The initial values of the PV parameters for the devices tested for stability are reported in Supplementary Table 6. It was found that the T_{80} lifetime of the PSMs is estimated to be 24, 116 and 268 h, respectively. The significantly improved device stability for the modules with both EDTAK and EAI/MAI treatment is ascribed to the above-mentioned ETL/perovskite and perovskite/HTL interface stabilization strategy.

Stabilization of the HTL/electrode interface

A stable HTL/electrode interface is also important for PSM stability.[41] To further improve the stability of HTL, we incorporated a small amount of P3HT into spiro-OMeTAD.[42] This mixed HTL (denoted as spiro-OMeTAD-P3HT) can deliver comparable performance with the spiro-OMeTAD based PSM (Supplementary Figure 19 and 20, Supplementary Table 6). To study whether this strategy can improve the stability, we measured the operation stability of PSM based on mixed HTL (SnO_2-EDTAK/PVSK(EAMA)/spiro-OMeTAD-P3HT/Au). It was found that the module with both EDTAK and EAI/MAI treatment and mixed HTL shows a T_{80} lifetime exceeding 1600 h, which is much longer than the pure spiro-OMeTAD case (Figure 5c). We ascribe the improved stability to the HTL/CE interface engineering, where the spiro-OMeTAD-P3HT layer may slow down the gold inward migration and also enhance the stability of HTL against moisture. To verify this, we performed SIMS measurements on the aged samples (Supplementary Figure 21). The SIMS results coherently indicate that the slower Au migration into spiro-OMeTAD-P3HT versus spiro-OMeTAD case, which slow down the irreversible degradation induced by Au migration.[40] The improved shielding effect of the spiro-OMeTAD-P3HT is assigned to the thiophene-like structures of P3HT that has a strong chemical interaction with Au, which helps retard Au migration (Supplementary Figure 22 and Supplementary Note 5).

In addition, moisture resistance of the HTLs was studied by measuring the contact angle of a deionized water droplet. The contact angle is increased from 71.6° for the spiro-OMeTAD sample to 107.0° for the spiro-OMeTAD-P3HT sample (Supplementary Figure 23). This observation evidently demonstrates a change of HTL from hydrophilic to hydrophobic through introducing additional conjugated polymers, i.e., P3HT into spiro-OMeTAD. The improved moisture resistance is beneficial for the device resistance against moisture during P2 cutting process and device operation. Note that when water droplets were kept on the top of spiro-OMeTAD-P3HT layer for several minutes during the contact angle test, the underneath perovskite still changed its color from dark brown to yellow, which suggests the spiro-OMeTAD-P3HT is not

able to completely retard the moisture induced degradation. This observation inspired us to make additional interface stabilization to further improve the PSMs stability.

Device encapsulation

To further improve PSMs stability, parylene encapsulation[43] and cover glass protection are employed on PSMs with both EDTAK and EAI/MAI treatment and mixed HTL (Supplementary Figure 24-26). The encapsulated PSMs show a comparable efficiency as PSMs without encapsulation (Supplementary Figure 27).

The operation stability of three encapsulated PSMs was investigated (Figure 5d and Supplementary Figure 28), and the temperature on the surface of the module was measured to be approximately 40 ^{o}C during stability measurements (Supplementary Figure 29). All three modules show nearly identical stability evolution trend. At the beginning, there is a very fast burn-in decay process. This might due to the thermal effect, a faster perovskite degradation or spiro-OMeTAD conductivity variation (Supplementary Note 6). We then observed a slightly increase of the performance followed by a slow linear decay, where the slow increase after burn-in decay is likely due to the perovskite recovery or spiro-OMeTAD conductivity recovery (Supplementary Note 6). Figure 5d shows that the encapsulated PSM with the best stability remained 86% of the initial performance after aging for 2000 h, and gave a T_{90} lifetime of 1570 h and an estimated T_{80} lifetime of 2680 h.[31] Moreover, all three modules show a T_{80} lifetime over 2000 h with good stability reproducibility, which give an average T_{80} lifetime of 2457±274 h.

Here, the parylene encapsulation is demonstrated to act as a thin-film barrier largely to enhance the long-term stability of PSMs (Supplementary Note 7). The thermal stability (60 ^{o}C) of the PSMs was also studied. The PSMs retained over 80% of their initial efficiency after 1000 h test (Supplementary Figure 30 and Supplementary Table 8). When compared with the reported results, our modules performance result is among the top reported efficiency and stability for PSMs (Supplementary Table 9). Our PSMs stability study suggests the relatively good

stability of our solar module and verify the effectiveness of above studied HIS strategy.

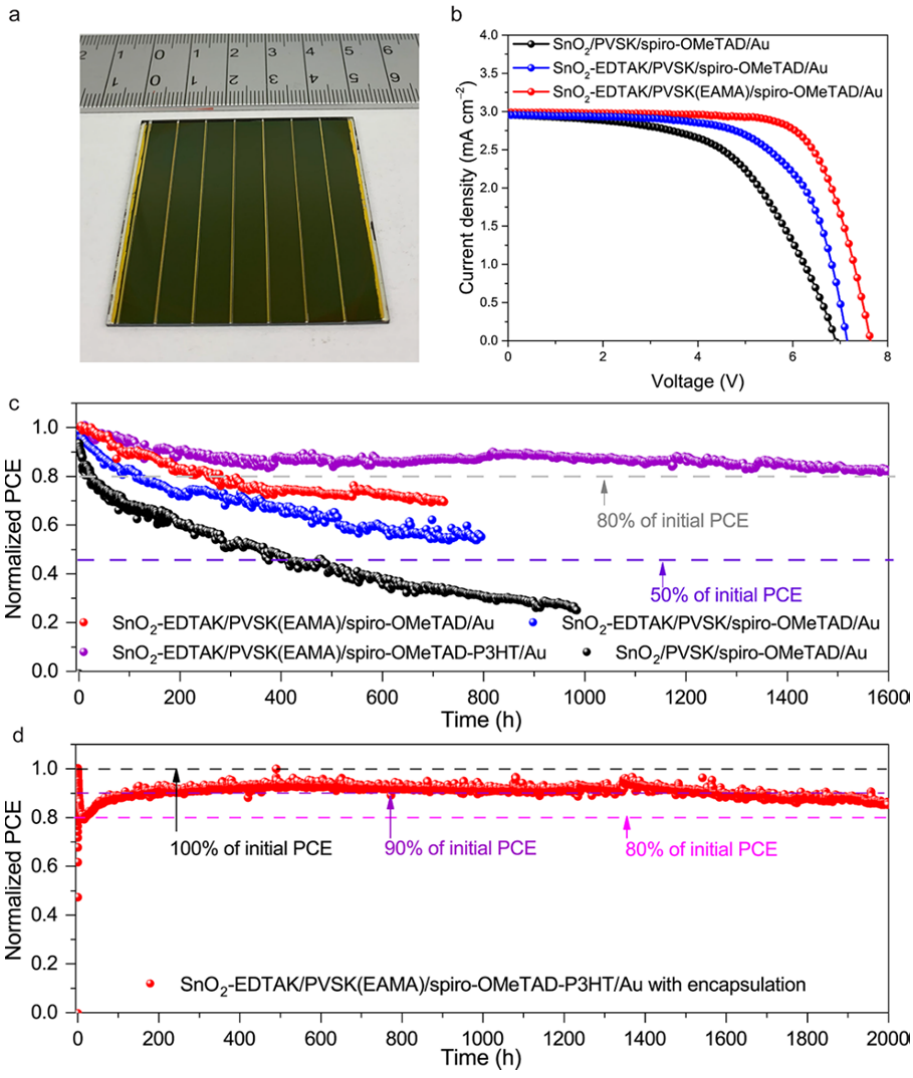

Figure 5 PSMs photovoltaic performance and stability. a, Photograph of a PSM. **b**, Representative J–V curves of the PSMs with varying structures. **c**, Operation stability of un-encapsulated PSMs with varying structures measured at a fixed bias near initial maximum power point (MPP) under continuous AM 1.5G light illumination in a N_2 box with a relative humidity <5%. The initial values of the PV parameters for the devices tested for stability are reported in Supplementary Table 6. **d**, Operation stability of encapsulated SnO_2-EDTAK/PVSK(EAMA)/spiro-OMeTAD-P3HT/Au PSM with parylene and a cover glass measured under the same conditions as in (**b**). The initial values of the PV parameters for the PSM tested for stability are reported in Supplementary Figure 27, PSM #1.

Conclusions

In summary, we demonstrated a holistic interface engineering strategy to fabricated PSMs relying on treatments that are compatible with scalable processing and scribing steps. First, we treated the SnO_2 ETL with EDTAK to mitigate the reaction of OH^- with perovskite, passivate defects and afford good energy-level alignment at the ETL/perovskite interface. Then, we passivated surface defects at the perovskite/HTL surface with ethylammonium iodide as well as improved perovskite stability and energy-level alignment at the perovskite/HTL interface. We then improved the device stability by incorporating P3HT into the HTL and encapsulate the device with a parylene film. The resultant PSMs without encapsulation achieved a reverse-scan efficiency of 16.6% with a designated area 22.4 cm^2. Moreover, the encapsulated PSM stability maintained about 86% of the initial performance after continuous operation for 2000 h under AM 1.5G light illumination, which translates into a T_{90} lifetime of 1570 h and a T_{80} lifetime of 2680 h. This demonstration is a step forwards in the development and commercialization of large-scale perovskite photovoltaics.

Methods

Materials. All reagents were used as received without further purification, including PbI_2 (99.99%, TCI), formamidinium iodide (FAI, greatcell solar), methylammonium iodide (MAI, greatcell solar), methylammonium bromide (MABr, greatcell solar), methylammonium chloride (MACl, greatcell solar), ethylammonium iodide (EAI, Sigma-Aldrich), cesium iodide (Sigma-Aldrich), 4-tert-butylpyridine (99.9%, Sigma Aldrich), bis(trifluoromethane)sulfonimide lithium salt (Li-TFSI, Sigma-Aldrich), acetonitrile (99.9%, Sigma-Aldrich), chlorobenzene (99.8%, Wako), 2,2′,7,7′-tetrakis(N,N-di-p-methoxyphenylamine)-9,9′-spirobifluorene (spiro-OMeTAD, Merck), poly(3-hexylthiophene) (P3HT, Luminescence Technology Corp.), SnO_2 (Alfa Aesar, tin (IV) oxide, 15% in H_2O colloidal dispersion), ethylenediaminetetraacetic acid dipotassium (Sigma-Aldrich), methanol (Wako),

isopropanol (Wako), N,N-dimethylformamide (DMF, Wako), dimethyl sulfoxide (DMSO, Wako).

PSCs fabrication. The ITO substrate was sequentially washed with distilled water, acetone, ethanol and isopropanol. Then treated using UV/O_3 for 30 min. The SnO_2 layer was subsequently coated on ITO substrate with the SnO_2 nanocrystal solution (diluted by H_2O to 2.5%) at 3000 rpm for 30 s, and annealed at 150 °C for 30 min in air. Then an ethylenediaminetetraacetic acid dipotassium methanol solution was spin-coated on the SnO_2 film at 3000 rpm for 30 s, and annealed at 100 °C for 5 min in air. Then, a 1.35 M PbI_2 and 0.0675 M CsI solution (dissolved in mixed DMF/DMSO (V:V = 19:1) solvent and stirred at 70 ^oC for 2 hours before filtered with PTFE syringe filters) was spin-coated on substrate at 2000 rpm for 30 s. Then a mixed organic cation solution (FAI 400 mg; MAI 200 mg; MABr 50 mg; MACl 50 mg, dissolved in 10 mL isopropanol) was spin-coated at 1750 rpm. for 30 s and then annealed at 150 °C for 15 min in air. Then a EAI/MAI solution dissolved in mixed IPA/DMF (V:V = 200:1) was spin-coated on the top of perovskite layer at 6000 rpm for 30 s and annealed at 70 ^oC for 5 min. Then the hole transport materials (HTM) solution was deposited by spin-coating at 3000 rpm for 30 s. The spiro-OMeTAD solution was prepared by dissolving spiro-OMeTAD in chlorobenzene (72.3 mg mL^{-1}) with the addition of 17.5 μL Li-TFSI/acetonitrile (520 mg mL^{-1}), and 28.8 μL 4-tert-butylpyridine. A mixture of spiro-OMeTAD/P3HT (weight ratio, 9:1) was used for mixed HTM solution preparation, similar amount of Li-TFSI and 4-tert-butylpyridine were added. Finally, a gold layer with a thickness of 100 nm was deposited as the counter electrode on the top of HTL through shadow masks via thermal evaporation under high vacuum (5×10^{-5} Torr).

PSMs fabrication. The perovskite solar module consists of seven perovskite sub-cells connected in series on a 5 cm × 5 cm substrate. Between each cell there is a line (P1) with a width of 50 μm patterned by laser-etching to separate ITO stripes, with a dimension of 6.65 mm by 49 mm (Supplementary Figure 14). The ETL, perovskite, and HTL were prepared using the same process as small-size PSCs. After

coating ETL, perovskite, and HTL, one more line (P2) with a width of about 250 μm is patterned by CO_2 laser with a power of 5.6 W to expose the bottom ITO/SnO_2 electrodes to form the series connections between the cells. A gold film with a thickness of 120 nm was then thermally evaporated as the counter electrode and each sub-cell was separated by mechanical scribing to form P3 patterning.

PSMs encapsulation. Parylene is used due to its robust water resistance capability and the capability to provide compact enclosure to prevent leakage. In addition, parylene encapsulation avoids the direct exposure of perovskite and HTL to air at the scribed series interconnections region in a PSM, which favors the enhancement of PSM stability. Before parylene encapsulation, metal wires were connected to the PSM by ultrasonic soldering (Sunbonder USM-560). Then, the parylene film was deposited by a chemical vapor deposition process using PDS 2010 LABCOATER (Supplementary Figure 24). The PSMs for encapsulation were first loaded into the CVD chamber, which was pumped to a pressure below 1500 Pa. Then, the precursor particles (Parylene C, SCS coatings, 2 g) were kept at a temperature of 175 ^{o}C for vaporization. The furnace tube is kept at a temperature of 690 ^{o}C to pyrolyse the precursor into monomers. During the parylene deposition, the chamber is kept at a pressure of approximately 3500 Pa. The substrate temperature during deposition was approximately 40 ^{o}C. The polymerization and deposition rate of parylene is approximately 2 μm per hour. The thickness of the parylene encapsulation was approximately 2 μm. A cover glass was further attached on the top of the PSMs to provide mechanical protection for the underneath layers. For cover glass sealing, a glass sheet with a thickness of 2 mm was carefully sealed on top of the parylene film by kapton tape (Supplementary Figure 25). The space between glass and the parylene film is approximately 0.2 mm, which is determined by the tape thickness.

Photovoltaic characterization. J–V characteristics of perovskite solar cells are measured under one sun illumination (AM 1.5 G, 100 mW cm^{-2}, calibrated using a KG3 reference Si-cell (Enlitech), Oriel Instruments Model Number 90026564, 2×2 cm^2) using a solar simulator (Newport Oriel Sol 1A, Xenon-lamp, USHIO,

UXL-150SO) and a Keithley 2420 source meter in ambient air at about 25 ^{o}C and a relative humidity of 40 ~ 60%. The small-size PSCs were measured using a metal mask with the aperture area of 0.09 cm^2. The designated area of 22.4 cm^2 for modules was defined by a corresponding metal mask. The J-V scan range is from −0.1 V to 1.2 V for small-size PSCs and from −0.2 V to 8.5 V for modules. All the J-V curves were measured under reverse scan with a scan rate of 0.25 V s^{-1} without preconditioning unless otherwise specified. No preconditioning protocol was used before the characterization. The EQE spectra of small-cells were characterized using Oriel IQE 200.

Stability testing. For continuous operation stability measurements, the PSMs were loaded in our home-designed enclosure box with dry N_2 flow to maintain a relative humidity below 5%. The PSMs were under continuous illumination by a solar simulator (Peccell PEC-L01, AM1.5G without UV filter) and source meter (Keithley 2401), which was controlled by a LabView program to allow automatic measurements on the PSMs. To simulate continuous PSM operation (i.e., operation stability), a fixed bias voltage was continuously applied to the PSMs maintaining the PSM operation near the MPP. The bias voltage value was set to be the initial MPP voltage during the operation stability measurement. The photocurrent output of the modules was also measured by Keithley 2401, and was recorded by the home-made LabView program. For the thermal stress test under dry N_2 condition, the PSMs were loaded on a hotplate at a temperature of approximately 60 ^{o}C for aging in a dry N_2 glove box with a relative humidity below 5%.

Characterization. SEM measurements were carried out using a scanning electron microscope (Helios NanoLab G3 UC, FEI). XRD measurements were carried out in a Bruker D8 Discover instrument (Bruker AXS GmbH, Karlsruhe, Germany) equipped with Cu wavelength λ = 1.54 Å X-ray source operated at 1600 W and Goebel mirror. The UPS and XPS spectra were recorded from an X-ray photoelectron spectrometer (XPS-AXIS UltranHAS, Kratos) equipped with monochromatic Al-Kα = 1486.6 eV and nonmonochromatic He–I = 21.22 eV sources. XPS results were

fitted using Gaussian-Lorentzian functions after background subtraction corresponding to the inelastic scattering processes. TRPL data were acquired using the time-correlated, single-photon counting technique (Hamamatsu, C10627), and excitation was provided by a femtosecond mode-locked Ti:sapphire laser (Spectra-Physics, MAITAI XF-IMW) at 450 nm with an average power at 8 MHz of 0.74 mW. SIMS (Kratos Axis ULTRA) equipped with quadrupole mass spectrometer (HAL 7, Hiden Analytical) was used to collect the elemental signal in positive ion detection mode (PID). For sputtering in SIMS, 3 keV Ar^+ primary beam with a current of 10 mA and a diameter of 100 μm was utilized. To study the effect of mixed HTM on retarding gold migration, we have prepared the samples according to a previous study on a similar topic.[40] Our result was obtained from the samples with Au layer. The samples were prepared on 1.5 cm × 1.5 cm ITO substrate according to the same procedure as the fabrication procedure of our devices. Then, the samples were placed on a hot plate which was kept at a temperature of 70 ^oC for 24 h in a N_2 glove box. The aged samples were transferred into the SIMS chamber for measurements. The beam was at an angle of 45 ° with respect to the sample surface normal. The spectrometer was operated at a pressure of 10^{-8} torr. The SCLC data were collected with a semiconductor characterization system in N_2 (4200-SCS, Keithley). Absorbance was measured using a UV-Vis spectrometer (JASCO Inc., V-670).

Reporting summary. Further information on research design is available in the Nature Research Reporting Summary linked to this article.

Data availability

All data generated or analysed during this study are included in the published article and its Supplementary Information. The data that support the plots within this article and other findings of this study are available from the corresponding author upon reasonable request.

Acknowledgements

This work was supported by funding from the Energy Materials and Surface Sciences Unit of the Okinawa Institute of Science and Technology Graduate

University, the OIST R&D Cluster Research Program, and the OIST Proof of Concept (POC) Program. We would like to thank OIST Mech. Eng. & Microfabrication Support Section for maintenance of cleanroom and parylene deposition equipment. The authors thank Dr. Mikas Remeika for writing the software for steady-state power measurements, Mr. Hyung Been Kang, Ms. Noriko Ishizu, Mr. Takuya Miyazawa and the Nanofab team for XRD, SEM, AFM and TRPL characterization.

Author contributions

Y.B.Q. supervised the project. Y.B.Q. and Z.L. conceived the ideas and designed the experiments. Z.L. conducted the corresponding device fabrication and basic characterization. Z.L. and L.Q. conducted module fabrication, encapsulation and stability testing. L.Q. and L.K.O. helped with XPS, UPS and SIMS characterization and analyses. S.H. helped with the module picture design and data analysis. Z.H. helped with energy alignment analyses. M.J. helped with TRPL characterization. G.T., Z.W., Y.J., Y.D., and S.K. provided valuable suggestions for the manuscript. S.K. contributed to the J-V characterization. Z.L. and Y.B.Q. participated in all the data analysis. All authors contributed to writing the paper.

Competing interests

All the authors declare no competing interests.

Additional information

Supplementary information is available for this paper at https://doi.org/

Correspondence and requests for materials should be addressed to Y.B.Q.

References

1 https://www.nrel.gov/pv/assets/pdfs/best-research-cell-efficiencies.20200218.pdf.

2 Li, Z. *et al.* Scalable fabrication of perovskite solar cells. *Nat. Rev. Mater.* **3**, 18017 (2018).

3 Kim, D. H., Whitaker, J. B., Li, Z., van Hest, M. F. A. M. & Zhu, K. Outlook and challenges of perovskite solar cells toward terawatt-scale photovoltaic module technology. *Joule* **2**, 1437-1451 (2018).

4 Qiu, L., He, S., Ono, L. K., Liu, S. & Qi, Y. B. Scalable fabrication of metal halide

perovskite solar cells and modules. *ACS Energy Lett.* **4**, 2147-2167 (2019).

5 Ono, L. K., Qi, Y. B. & Liu, S. Progress toward stable lead halide perovskite solar cells. *Joule* **2**, 1961-1990 (2018).

6 Correa-Baena, J.-P. *et al.* Promises and challenges of perovskite solar cells. *Science* **358**, 739-744 (2017).

7 Domanski, K., Alharbi, E. A., Hagfeldt, A., Grätzel, M. & Tress, W. Systematic investigation of the impact of operation conditions on the degradation behaviour of perovskite solar cells. *Nat. Energy* **3**, 61-67 (2018).

8 Saliba, M., Stolterfoht, M., Wolff, C. M., Neher, D. & Abate, A. Measuring aging stability of perovskite solar cells. *Joule* **2**, 1019-1024 (2018).

9 Khenkin, M. V. *et al.* Consensus statement for stability assessment and reporting for perovskite photovoltaics based on ISOS procedures. *Nat. Energy* **5**, 35-49 (2020).

10 Saliba, M. *et al.* Incorporation of rubidium cations into perovskite solar cells improves photovoltaic performance. *Science* **354**, 206-209 (2016).

11 Wang, Z. *et al.* Efficient ambient-air-stable solar cells with 2D–3D heterostructured butylammonium-caesium-formamidinium lead halide perovskites. *Nat. Energy* **6**, 17135, (2017).

12 Wang, L. *et al.* A Eu^{3+}-Eu^{2+} ion redox shuttle imparts operational durability to Pb-I perovskite solar cells. *Science* **363**, 265-270 (2019).

13 Bai, S. *et al.* Planar perovskite solar cells with long-term stability using ionic liquid additives. *Nature* **571**, 245-250 (2019).

14 Yang, S. *et al.* Stabilizing halide perovskite surfaces for solar cell operation with wide-bandgap lead oxysalts. *Science* **365**, 473-478 (2019).

15 Fang, R. *et al.* [6,6]-Phenyl-C61-Butyric acid methyl ester/cerium oxide bilayer structure as efficient and stable electron transport layer for inverted perovskite solar cells. *ACS Nano* **12**, 2403-2414 (2018).

16 Jung, E. H. *et al.* Efficient, stable and scalable perovskite solar cells using poly(3-hexylthiophene). *Nature* **567**, 511-515 (2019).

17 Wu, S. *et al.* A chemically inert bismuth interlayer enhances long-term stability of

610 inverted perovskite solar cells. *Nat. Commun.* **10**, 1161 (2019).

611 18 Cheacharoen, R. *et al.* Encapsulating perovskite solar cells to withstand damp heat
612 and thermal cycling. *Sustain. Energy Fuels* **2**, 2398-2406 (2018).

613 19 Yang, M. *et al.* Highly efficient perovskite solar modules by scalable fabrication
614 and interconnection optimization. *ACS Energy Lett.* **3**, 322-328 (2018).

615 20 Matteocci, F. *et al.* High efficiency photovoltaic module based on mesoscopic
616 organometal halide perovskite. *Prog. Photovolt: Res. Appl.* **24**, 436-445 (2016).

617 21 Bi, E. *et al.* Efficient perovskite solar cell modules with high stability enabled by
618 iodide diffusion barriers. *Joule* **3**, 1-13 (2019).

619 22 Bu, T. *et al.* Universal passivation strategy to slot-die printed SnO_2 for
620 hysteresis-free efficient flexible perovskite solar module. *Nat. Commun.* **9**, 4609 (2018).

621 23 Xu, Z. *et al.* A Thermodynamically favored crystal orientation in mixed
622 formamidinium/methylammonium perovskite for efficient solar cells. *Adv. Mater.* **31**, 1900390
623 (2019).

624 24 Jiang, Q. *et al.* Enhanced electron extraction using SnO_2 for high-efficiency
625 planar-structure $HC(NH_2)_2PbI_3$-based perovskite solar cells. *Nat. Energy* **1**, 16177 (2016).

626 25 Qiu, L. *et al.* Scalable fabrication of stable high efficiency perovskite solar cells
627 and modules utilizing room temperature sputtered SnO_2 electron transport layer. *Adv. Funct.*
628 *Mater.* **29**, 1806779 (2018).

629 26 Brinkmann, K. O. *et al.* Suppressed decomposition of organometal halide
630 perovskites by impermeable electron-extraction layers in inverted solar cells. *Nat. Commun.* **8**,
631 13938 (2017).

632 27 Yang, D. *et al.* High efficiency planar-type perovskite solar cells with negligible
633 hysteresis using EDTA-complexed SnO_2. *Nat. Commun.* **9**, 3239 (2018).

634 28 Li, X., Zhang, W., Wang, X., Gao, F. & Fang, J. Disodium edetate as a promising
635 interfacial material for inverted organic solar cells and the device performance optimization.
636 *ACS Appl. Mater. Interfaces* **6**, 20569-20573 (2014).

637 29 Son, D.-Y. *et al.* Universal approach toward hysteresis-free perovskite solar cell
638 via defect engineering. *J. Am. Chem. Soc.* **140**, 1358-1364 (2018).

30 Wu, W.-Q. *et al.* Bilateral alkylamine for suppressing charge recombination and improving stability in blade-coated perovskite solar cells. *Sci. Adv.* **5**, eaav8925 (2019).

31 Liu, Z. *et al.* Gas-solid reaction based over one-micrometer thick stable perovskite films for efficient solar cells and modules. *Nat. Commun.* **9**, 3880 (2018).

32 Im, J.-H., Chung, J., Kim, S.-J. & Park, N.-G. Synthesis, structure, and photovoltaic property of a nanocrystalline 2H perovskite-type novel sensitizer ($(CH_3CH_2NH_3)PbI_3$). *Nanoscale Res. Lett.* **7**, 353 (2012).

33 Peng, W. *et al.* Engineering of $CH_3NH_3PbI_3$ perovskite crystals by alloying large organic cations for enhanced thermal stability and transport properties. *Angew. Chem. Int. Ed.* **55**, 10686-10690 (2016).

34 Zhou, J. *et al.* Efficient ambient-air-stable HTM-free carbon-based perovskite solar cells with hybrid 2D–3D lead halide photoabsorbers. *J. Mater. Chem. A* **6**, 22626-22635 (2018).

35 Zhang, Y., Kim, S.-G., Lee, D., Shin, H. & Park, N.-G. Bifacial stamping for high efficiency perovskite solar cells. *Energy Environ. Sci.* **12**, 308-321 (2019).

36 Gholipour, S. *et al.* Globularity-selected large molecules for a new generation of multication perovskites. *Adv. Mater.* **29**, 1702005 (2017).

37 Wang, Y. *et al.* A mixed-cation lead iodide $MA_{1-x}EA_xPbI_3$ absorber for perovskite solar cells. *J. Energy Chem.* **27**, 215-218 (2018).

38 Luo, D. *et al.* Enhanced photovoltage for inverted planar heterojunction perovskite solar cells. *Science* **360**, 1442-1446 (2018).

39 Jiang, Y. *et al.* Combination of hybrid CVD and cation exchange for upscaling Cs-substituted mixed cation perovskite solar cells with high efficiency and stability. *Adv. Funct. Mater.* **28**, 1703835 (2017).

40 Domanski, K. *et al.* Not all that glitters is gold: metal-migration-induced degradation in perovskite solar cells. *ACS Nano* **10**, 6306-6314 (2016).

41 Christians, J. A. *et al.* Tailored interfaces of unencapsulated perovskite solar cells for >1,000 hour operational stability. *Nat. Energy* **3**, 68-74 (2018).

42 Kim, G.-W., Kang, G., Malekshahi Byranvand, M., Lee, G.-Y. & Park, T.

668 Gradated mixed hole transport layer in a perovskite solar cell: improving moisture stability
669 and efficiency. *ACS Appl. Mater. Interfaces* **9**, 27720-27726 (2017).
670 43 Jinno, H. *et al.* Stretchable and waterproof elastomer-coated organic photovoltaics
671 for washable electronic textile applications. *Nat. Energy* **2**, 780-785 (2017).
672